Proceedings of the Korean Nuclear Society Autumn Meeting
Pohang, Korea, May 1999

Development of a Three-Dimensional Thermal-Hydraulic Analysis Code for Thermally Stratified Flow in a Curved Piping System

Jong Chull Jo

Korea Institute of Nuclear Safety
19 Kusung-dong, Yusung-ku, Taejon 305-338, Korea

Seok Ki Choi

Korea Atomic Energy Research Institute
150 Dukjin-dong, Yusung-ku, Taejon 305-353, Korea

Abstract

A three-dimensional thermal-hydraulic code for analyzing the thermally stratified flows in a curved piping system has been developed by using body-fitted non-orthogonal curvilinear coordinates. The transient behaviors of stratified fluid flow are simulated using the finite volume approach. The convection term is approximated by a higher-order bounded scheme named COPLA, which is known as a high-resolution and bounded discretization scheme. The cell-centered, non-staggered grid arrangement is adopted and the resulting checkerboard pressure oscillation is prevented by the application of modified momentum interpolation scheme. The SIMPLE algorithm is employed for the pressure and velocity coupling. The thermal-hydraulic code developed in this study has been validated by the comparison of the predicted results with the available experimental data. As a result, the predictions with the code developed in the present study have shown to be in good agreement with the experimental results.

1. Introduction

Some safety-related piping systems connected to reactor coolant systems at operating nuclear power plants are known to be potentially susceptible to unanticipated flow-induced thermal stratification which can lead to thermal fatigue damage to the piping systems. Several plants have so far experienced such serious mechanical damages due to thermal fatigue as pressurizer surgeline movements and its support failures, and cracks in feedwater nozzle, high pressure safety injection lines, and residual heat removal lines. Thus, the USNRC has provided generic commuications[1-4] to its licensees addressing safety issues arising from thermal stresses and fatigue caused by thermal stratification. Toasses the potential for piping damage due to the thermal stratification, it is necessary, first of all, to predict accurately the thermally stratified flows.

Several investigators[5-9] have made efforts to determine the temperature distributions in the pipe wall by means of laboratory testing of a particular geometry or field measurement of temperatures or fully theoretical predictions. Difficulties and limitations in applying the first two approaches for operating plants lead to depend on the predictions by numerical analyses. Most literatures addressing the theoretical predictions are based on the two-dimensional analyses are available. In many practical problems, the piping systems have complicated shaped boundaries surrounding the buoyancy-influenced thermally stratified flows. This makes the multi-dimensional numerical analyses difficult. Ushijima[10] has provided a numerical method for predicting thermal stratification in a curved duct with three-dimensional body-fitted coordinates, utilizing a Lagrangian scheme, and has performed experiment to measure the thermally stratified flow parameters in the curved duct such as velocity distributions, secondary flow patterns, and temperature profiles for the comparative study.

In the present study, a three-dimensional thermal-hydraulic code for analyzing the thermally stratified flows in curved piping systems has been developed by using body-fitted non-orthogonal curvilinear coordinates. The transient behaviors of stratified fluid flow are simulated using the finite volume approach. The convection term is approximated by a higher-order bounded scheme named COPLA[11], which is known as a high-resolution and bounded discretization scheme. The cell-centered, non-staggered grid arrangement is adopted and the resulting checkerboard pressure oscillation is prevented by the application of modified momentum interpolation scheme[12]. The SIMPLE algorithm[13] is employed for the pressure and velocity coupling.

The thermal-hydraulic code developed in this study has been validated by the comparison of the predicted results with the available experimental data. As a result, the predictions with the code developed in the present study have shown to be in good agreement with the experimental results.

2. Mathmatical formulation

Governing Equations

For simplicity, it is assumed the thermally stratified fluids are Newtonian with constant properties and the Boussinesq approximation is valid. Then the governing equation of this thermally stratified flow inside the pipewith an arbitrarily shaped boundaries can be expressed in a generalized coordinate system x^j as,

Mass conservation equation

$$\frac{\partial}{\partial x^1}U_1+\frac{\partial}{\partial x^2}U_2+\frac{\partial}{\partial x^3}U_3=0 \tag{1}$$

where $$U_i = r\,u_k b_k^i \tag{2}$$

where u_k denotes the three Cartesian velocity components in the directions of the transformed coordinates $y^i = y^i(x^j)$. and the geometric coefficients b_i^j represent the cofactors of $\partial y^i/\partial x^j$ in the Jacobian matrix of the coordinate transformation, J stands for the determinant of the Jacobian matrix and y^i is the Cartesian coordinate system.

Momentum equations

$$\begin{aligned}&\frac{\partial}{\partial t}(Jru_1)+\frac{\partial}{\partial x^1}\left[U_1u_1-\frac{m}{J}\left\{\frac{\partial u_1}{\partial x^1}B_1^1+\frac{\partial u_1}{\partial x^2}B_2^1+\frac{\partial u_1}{\partial x^3}B_3^1+b_1^1w_1^1+b_2^1w_1^2+b_3^1w_1^3\right\}+Pb_1^1\right]\\&+\frac{\partial}{\partial x^2}\left[U_2u_1-\frac{m}{J}\left\{\frac{\partial u_1}{\partial x^1}B_1^2+\frac{\partial u_1}{\partial x^2}B_2^2+\frac{\partial u_1}{\partial x^3}B_3^2+b_1^2w_1^1+b_2^2w_1^2+b_3^2w_1^3\right\}+Pb_1^2\right]\\&+\frac{\partial}{\partial x^3}\left[U_3u_1-\frac{m}{J}\left\{\frac{\partial u_1}{\partial x^1}B_1^3+\frac{\partial u_1}{\partial x^2}B_2^3+\frac{\partial u_1}{\partial x^3}B_3^3+b_1^3w_1^1+b_2^3w_1^2+b_3^3w_1^3\right\}+Pb_1^3\right]=r\,g\,b\,(T-T_{ref})J\end{aligned} \tag{3a}$$

$$\begin{aligned}&\frac{\partial}{\partial t}(Jru_2)+\frac{\partial}{\partial x^1}\left[U_1u_2-\frac{m}{J}\left\{\frac{\partial u_2}{\partial x^1}B_1^1+\frac{\partial u_2}{\partial x^2}B_2^1+\frac{\partial u_2}{\partial x^3}B_3^1+b_1^1w_2^1+b_2^1w_2^2+b_3^1w_2^3\right\}+Pb_2^1\right]\\&+\frac{\partial}{\partial x^2}\left[U_2u_2-\frac{m}{J}\left\{\frac{\partial u_2}{\partial x^1}B_1^2+\frac{\partial u_2}{\partial x^2}B_2^2+\frac{\partial u_2}{\partial x^3}B_3^2+b_1^2w_2^1+b_2^2w_2^2+b_3^2w_2^3\right\}+Pb_2^2\right]\\&+\frac{\partial}{\partial x^3}\left[U_3u_2-\frac{m}{J}\left\{\frac{\partial u_2}{\partial x^1}B_1^3+\frac{\partial u_2}{\partial x^2}B_2^3+\frac{\partial u_2}{\partial x^3}B_3^3+b_1^3w_2^1+b_2^3w_2^2+b_3^3w_2^3\right\}+Pb_2^3\right]=0\end{aligned} \tag{3b}$$

$$\begin{aligned}&\frac{\partial}{\partial t}(Jru_3)+\frac{\partial}{\partial x^1}\left[U_1u_3-\frac{m}{J}\left\{\frac{\partial u_3}{\partial x^1}B_1^1+\frac{\partial u_3}{\partial x^2}B_2^1+\frac{\partial u_3}{\partial x^3}B_3^1+b_1^1w_3^1+b_2^1w_3^2+b_3^1w_3^3\right\}+Pb_3^1\right]\\&+\frac{\partial}{\partial x^2}\left[U_2u_3-\frac{m}{J}\left\{\frac{\partial u_3}{\partial x^1}B_1^2+\frac{\partial u_3}{\partial x^2}B_2^2+\frac{\partial u_3}{\partial x^3}B_3^2+b_1^2w_3^1+b_2^2w_3^2+b_3^2w_3^3\right\}+Pb_3^2\right]\\&+\frac{\partial}{\partial x^3}\left[U_3u_3-\frac{m}{J}\left\{\frac{\partial u_3}{\partial x^1}B_1^3+\frac{\partial u_3}{\partial x^2}B_2^3+\frac{\partial u_3}{\partial x^3}B_3^3+b_1^3w_3^1+b_2^3w_3^2+b_3^3w_3^3\right\}+Pb_3^3\right]=0\end{aligned} \tag{3c}$$

where

$$B_m^j = b_k^j\,b_k^m\,, \qquad w_j^i=\frac{\partial u_i}{\partial x^k}\,b_j^k \tag{4}$$

Energy equation

$$\frac{\partial}{\partial t}(Jr\,C_pT)+\frac{\partial}{\partial x^1}\left[U_1C_pT-\frac{k}{J}\left\{\frac{\partial T}{\partial x^1}B_1^1+\frac{\partial T}{\partial x^2}B_2^1+\frac{\partial T}{\partial x^3}B_3^1\right\}\right]$$

$$+\frac{\partial}{\partial x^2}\left[U_2 C_p T - \frac{k}{J}\left\{\frac{\partial T}{\partial x^1} B_1^2 + \frac{\partial T}{\partial x^2} B_2^2 + \frac{\partial T}{\partial x^3} B_3^2\right\}\right]$$

$$+\frac{\partial}{\partial x^3}\left[U_3 C_p T - \frac{k}{J}\left\{\frac{\partial T}{\partial x^1} B_1^3 + \frac{\partial T}{\partial x^2} B_2^3 + \frac{\partial T}{\partial x^3} B_3^3\right\}\right] = 0 \qquad (5)$$

In the above equations (1) - (5), ρ, μ, p, k, c_p, β, g and T denote respectively density, viscosity, pressure, thermal conductivity, specific heat, volumetric coefficient of thermal expansion, the gravitational acceleration and temperature. In addition, T_{ref} is the reference temperature.

Initial and Boundary Conditions

Consider a general situation of thermally stratified flow in a curved piping system with arbitrarily shaped boundaries where a fluid of the specified initial temperature is flowing through the piping system at constant flowrate so that the steady flow condition is maintained, and then the flow condition is changed at any point of time.

Because the solution domain is symmetrical thermally and geometrically, only half of the region is needed to analyze. Thus along the symmetry line, the symmetry boundary conditions will be applied for both velocity and temperature. On the solid wall, no slip and adiabatic boundary conditions are specified, so that the velocity of fluid vanishes. For this situation the boundary conditions are given by

$u_i = u_{i,in}$, $T = T_{in}$ $(i = 1, 2, 3)$ at the inlet of the pipe, $t > 0$ (6a)

$u_i = 0$ $(i = 1, 2, 3)$, $\left.\frac{\partial T}{\partial n}\right|_{x^2} = \left.\frac{\partial T}{\partial n}\right|_{x^3} = 0$ at the inner surface of the pipe, $t > 0$ (6b)

$u_2 = 0$, $\frac{\partial u_1}{\partial x^2} = \frac{\partial u_3}{\partial x^2} = 0$, $\frac{\partial T}{\partial x^2} = 0$ at the symmetry plane, $t > 0$ (6c)

$\frac{\partial u_1}{\partial x^1} = \frac{\partial u_2}{\partial x^1} = \frac{\partial u_3}{\partial x^1} = 0$, $\frac{\partial T}{\partial x^1} = 0$ at the outlet of the pipe, $t > 0$ (6d)

3. Numerical method of solution

Solution Domain Discretization

The governing equations (1) – (5) are solved numerically by a finite volume approach, requiring the discretization of the solution domain into a finite number of hexahedral control volume cell whose faces are coincided with the non-orthogonal curvilinear coordinate lines. The values of all computed variables are stored at the geometric center of each control volume cell. The numerical grids are generated for a half symmetric region of the solution domain by using an algebraic method

Discretization of Governing Equation

In this study, the discretization of the governing equations is performed following the finite volume approach, and the convection terms are approximated by the COPLA scheme developed by Choi et al.[11] and the unsteady term is treated by the backward differencing scheme. The resulting algebraic equation for a variable ϕ can be written in the following general form.

$$A_P \phi_P = A_E \phi_E + A_W \phi_W + A_N \phi_N + A_S \phi_S + A_T \phi_T + A_B \phi_B + b_\phi \qquad (7)$$

where A_j $(j = P, E, W, N, S, T \text{ and } B)$ are coefficients and b_ϕ is a source term for variable ϕ.

Momentum Interpolation Method

For a better resolution of flow field in complex geometries, recently several investigators have developed various calculation methods of momentum equations employing the non-orthogonal, body-fitted coordinates. Among these methods, the non-staggered, momentum interpolation method originally developed by Rhie and Chow [14] is known to be one of the efficient methods and has been widely used because of its simplicity feature of algorithm. In this method, the momentum equations are solved at the cell centered locations using the Cartesian velocity components as dependent variables and the cell face velocities are obtained through the interpolation of the momentum equations for the neighboring cell centered Cartesian velocity components. In the present study, a modified version of the Rhie and Chow's scheme is proposed to obtain a converged solution of unsteady flows which is independent of the size of time step and relaxation factors.

The momentum equations solved implicitly at the cell centered location in the Rhie and Chow's scheme. The discretized momentum equations for cell centered velocity components can be written in terms of the under-relaxation factors expressed explicitly as follows:

$$u_{1,P} = (H_{u_1})_P + (D^1_{u_1})_P (P_w - P_e)_P + (D^2_{u_1})_P (P_s - P_n)_P + (D^3_{u_1})_P (P_b - P_t)_P + (E_{u_1})_P u^{n-1}_{1,P} + (1-\alpha_{u_1}) u^{l-1}_{1,P} \quad (8a)$$

$$u_{2,P} = (H_{u_2})_P + (D^1_{u_2})_P (P_w - P_e)_P + (D^2_{u_2})_P (P_s - P_n)_P + (D^3_{u_2})_P (P_b - P_t)_P + (E_{u_2})_P u^{n-1}_{2,P} + (1-\alpha_{u_2}) u^{l-1}_{2,P} \quad (8b)$$

$$u_{3,P} = (H_{u_3})_P + (D^1_{u_3})_P (P_w - P_e)_P + (D^2_{u_3})_P (P_s - P_n)_P + (D^3_{u_3})_P (P_b - P_t)_P + (E_{u_3})_P u^{n-1}_{3,P} + (1-\alpha_{u_3}) u^{l-1}_{3,P} \quad (8b)$$

where
$$H_{u_i} = \alpha_{u_i} \left\{ \sum A^{u_i}_{nb} u_{i,nb} + (S^{u_i}_c \Delta V) \right\} \Big/ A^{u_i}_P$$
$$D^j_{u_i} = \alpha_{u_i} b^j_i / A^{u_i}_P, \quad E_{u_i} = \frac{\alpha_{u_i} \rho \Delta V}{\Delta t} \Big/ A^{u_i}_p \qquad (i = 1, 2, 3) \quad (9)$$
$$A^{u_i}_P = \sum A^{u_i}_{nb} - S^{u_i}_P \Delta V + \frac{\rho \Delta V}{\Delta t}$$

and $\alpha_{u_i} (i = 1, 2, 3)$ are the under relaxation factors for u_1, u_2, u_3 velocity components and the superscripts $n-1$, $l-1$ denote the previous time step and iteration level, respectively. The discretized form of momentum equations for the cell face velocity component, for example at the east face, can be written as follows.

$$u_{1,e} = (H_{u_1})_e + (D^1_{u_1})_e (P_P - P_E) + (D^2_{u_1})_e (P_{se} - P_{ne}) + (D^3_{u_1})_e (P_{be} - P_{te}) + (E_{u_1})_e u^{n-1}_{1,e} + (1-\alpha_{u_1}) u^{l-1}_{1,e} \quad (10a)$$

$$u_{2,e} = (H_{u_2})_e + (D^1_{u_2})_e (P_P - P_E) + (D^2_{u_2})_e (P_{se} - P_{ne}) + (D^3_{u_2})_e (P_{be} - P_{te}) + (E_{u_2})_e u^{n-1}_{2,e} + (1-\alpha_{u_2}) u^{l-1}_{2,e} \quad (10b)$$

$$u_{3,e} = (H_{u_3})_e + (D^1_{u_3})_e (P_P - P_E) + (D^2_{u_3})_e (P_{se} - P_{ne}) + (D^3_{u_3})_e (P_{be} - P_{te}) + (E_{u_3})_e u^{n-1}_{3,e} + (1-\alpha_{u_3}) u^{l-1}_{3,e} \quad (10c)$$

In the present modified Rhie and Chow's scheme, this cell face (the east face) velocity component is obtained explicitly through the interpolation of momentum equations for the neighboring cell centered Cartesian velocity components. Following assumptions are introduced to evaluate these east cell face velocity components. For example, the assumptions for evaluation of the cell face velocity component u_1 can be expressed as follows:

$$(H_{u_1})_e \approx f^+_e (H_{u_1})_E + (1 - f^+_e)(H_{u_1})_P \quad (11)$$

$$(D^2_{u_1})_e (P_{se} - P_{ne}) \approx f^+_e (D^2_{u_1})_E (P_s - P_n)_E + (1 - f^+_e)(D^2_{u_1})_P (P_s - P_n)_P \quad (12)$$

$$(D^3_{u_1})_e (P_{be} - P_{te}) \approx f^+_e (D^3_{u_1})_E (P_b - P_t)_E + (1 - f^+_e)(D^3_{u_1})_P (P_b - P_t)_P \quad (13)$$

$$\frac{1}{(A^{u_1}_P)_e} \approx \frac{f^+_e}{(A^{u_1}_P)_E} + \frac{(1 - f^+_e)}{(A^{u_1}_P)_P} \quad (14)$$

where f^+_e is the geometric interpolation factor defined in terms of distances between nodal points. Similar assumptions can be introduced for evaluation of the velocity component at the north and top faces.

Using above assumption, the velocity component $u_{1,e}$ can be obtained as follows:

$$u_{1,e} = \left[f^+_e u_{1,E} + (1 - f^+_e) u_{1,p} + (D^1_{u_1})_e (P_p - P_E) - f^+_e (D^1_{u_1})_E (P_w - P_e)_E - (1 - f^+_e)(D^1_{u1})_P (P_w - P_e)_P \right]$$
$$+ (1 - \alpha_{u_1}) \left[u^{l-1}_{1,e} - f^+_e u^{l-1}_{1,E} - (1 - f^+_e) u^{l-1}_{1,P} \right] + \frac{\alpha_{u_1} \rho}{\Delta t} \left[\frac{(\Delta V)_e}{(A^{u_1}_P)_e} u^{n-1}_{1,e} - f^+_e \frac{(\Delta V)_E}{(A^{u_1}_P)_E} u^{n-1}_{1,E} - (1 - f^+_e) \frac{(\Delta V)_P}{(A^{u_1}_P)_P} u^{n-1}_{1,P} \right] \quad (15)$$

The term in the first bracket of right hand side of Eq. (15) is the original Rhie and Chow's scheme. Majumdar[15] has revealed that the converged solution is relaxation factor dependent if the term in the second bracket is omitted. For the same reason, omission of the term in the last bracket leads to the converged solution that is dependent on the size of time step as well as the relaxation factors. To the present author's knowledge, nobody has mentioned in the literature the last term, which comes from the unsteady term. Although the above two terms are relatively small in practical calculations and do not influence the accuracy of the converged solution significantly, this features that the converged solution is dependent on the relaxation factors and the size of time step are obviously undesirable. Eq. (15) indicates that the previous time step and iteration values of cell face velocity components as well as those of centered velocity components should be stored in order to obtain converged solutions which are independent of the size of time step and relaxation factors.

4. Results and discussions

Calculations are performed for the thermally stratified flow in a curved duct as shown in Fig.1, experimentally conducted by Ushijima[10]. The 84×17×34 numerical grids are generated using the algebraic method, and are shown in Fig.2. Only the symmetric half of the duct is solved. The Reynolds number based on the hydraulic diameter and the inlet velocity is 500 and the Richardson number is 9.8. Since the Richardson number is relatively high, the buoyancy force strongly affects the flow field. First, the steady state solutions are obtained with the temperature maintained at high temperature. The transient solution is obtained using the steady solution as an initial condition. The inlet temperature is assumed to be lowered linearly 10 degrees during the first 30 seconds, which approximately simulates the experimental condition. Calculations are continued until 120 seconds using the time step of 0.1 sec. The convergence is declared at each time step when the maximum of the absolute sum of the residuals of momentum equations, pressure correction equation and energy equation is less than 10^{-4}.

Figure 3 presents the comparision of experimentally measured results and calculated results for isothermal lines at the symmetry plane. The temperatures are normalized using the hot temperature and the cold temperature and the interval of the isothermal lines is 0.1. Relatively good agreements are obtained, and the discrepancy between the measured and calculated results may be partly due to the difference in experimental condition and imposed calculation condition. It is observed that the high temperature region is early formed and is not well mixed with the cold temperature fluid. After about 70 seconds, the stratification is established and even after 120 seconds, the stratification is not much varied and the numerically predicted features fairly well agree with the experimental results.

Figure 4 displays the predicted velocity field at the symmetry plane. It is observed that there exists a counterclockwise vortex appears at the upper region of the curved duct and the vortex disappears as time elapses. There also exists a recirculating flow at the downstream of the curved duct in the earlier stage of mixing process. The natural convection due to flowing of the cold temperature to the hot temperature fluid may be the main cause of this phenomenon. As time elapses, the fluid motion in the hot temperature region is very weak and the cold fluid in the bottom region of the duct moves fast.

Figure 5 shows the secondary motion in a duct at three different locations, sections A, B and C shown in Fig.1. There exists a relatively strong vortex at t=0 and the vortex becomes weak as the mixing process continues. The strength of secondary motion in the cold fluid region is relatively strong compared with those of hot fluid region. Their magnitude is not much different in the initial stage of mixing process. After the stratification is established (after 70 sec), the secondary motion in hot fluid region is very weak and there exists a strong clockwise vortex at the right-bottom corner of the duct at the sections A and B.

Figure 6 shows the predicted isothermal lines at the sections A, B and C. This figure shows well the development of stratification process. At the earlier stage of the mixing process, the temperature gradient is small and becomes steep as the stratification established. The steep gradient of temperature field hampers the mixing process and is not changed even the time elapses. A stable stratification is established at t=120 sec.

The present calculation method well predicts the thermal stratification phenomenon in a curved duct. The predicted temperature field well agrees with the experimentally measured results. The present method can be applied to the prediction of thermal stratification in a various piping systems, especially that of the pressure surge line in the pressuried water reactor.

5. Conclusions

An efficient numerical method for calculating the thermally stratified flows in a curved duct has been presented. The method employs a body-fitted non-orthogonal grid system to accommodate the shape of the duct and the interface of two fluids at different temperatures of which the level is variable, in the calculations.

The transient behaviors of fluid flow and temperature distribution in a piping were simulated using the finite volume approach. The convection term is approximated by a higher-order bounded scheme named COPLA, which is known to be a high-resolution and bounded discretization scheme. The cell-centered, non-staggered grid arrangement is adopted and the resulting checkerboard pressure oscillation is prevented by the application of modified momentum interpolation scheme. The SIMPLE algorithm is employed for the pressure and velocity coupling.

The method proposed in this study was applied to the thermal stratification in a curved duct, and the results have been discussed in detail. The results showed that the present method is applicable for the prediction of thermal stratification problem.

Although this paper addressed only one special case, it is emphasized that the present method can be extended for applications to various cases of thermally stratified flows in pipes and tanks with complex geometry and different flow conditions.

References

[1] US NRC Bulletin 79-13, Cracking in Feedwater System Piping.
[2] US NRC Bulletin 88-08, Thermal Stress in Piping Connected to Reactor Coolant System.
[3] US NRC Bulletin 88-11, Pressurizer Surge Line Thermal Stratification.
[4] US NRC NUREG/CR-6456, Review of Industry Efforts to Manage Pressurized Water Reactor Feedwater Nozzle, Piping, and Feedring Cracking and Wall Thinning.
[5] Smith, W.R., et al. (1988), "A solution for the Temperature Distribution in a Pipe Wall Subjected to Internally Stratified Flow," Proceedings of the 1988 Joint ASME-ANS Nuclear Power Conf., Myrtle Beach, South Carolina, pp. 45-50.
[6] Talja, A., and Hansjosten, E. (1990), "Results of Thermal Stratification Tests in a Horizontal Pipe Line at the HDR-Facility," Nucl. Eng. and Design, Vol. 118, pp.29-41.
[7] Ensel, C., et al. (1995), "Stress Analysis of a 900 MW Pressurizer Surge Line Including Stratification Effects," Nucl. Eng. and Design 153, 197-203.
[8] Jung, I.S., et al. (1996), "Thermal Stratification in a Horizontal Pipe of Pressurizer Surge Line," Transactions of KSME; B, Vol.20, No.4, 1449-1457.
[9] Yu, Y.J., et al. (1997), "Structural Evaluation of Thermal Stratification for PWR Surge Line," Nucl. Eng. and Design 178, 211-220.
[10] Ushijima. S. (1994), "Prediction of Thermal Stratification in a Curved Duct with 3D Body-Fitted Co-ordinates," Int'l J. for Numerical Methods in Fluids, Vol.19, pp.647-665.
[11] Choi, S. K., Nam, H. Y. and Cho, M. (1995), "Evaluation of a Higher-Order Bounded Scheme: Three- Dimensional Numerical Experiments," Numerical Heat Transfer, Part B, Vol. 28, pp. 23-28.
[12] Jo, J. C., Kim, Y. I. and Choi, S. K., "Heat Transfer Analysis of Thermal Stratification in Piping Connected to Reactor Coolant System.": in Proc. of the 1st Korea-Japan Symposium on Nuclear Thermal Hydraulics and Safety, Paper No. WR-13, pp.191-198, 1998.
[13] Patankar, S. V. (1980), Numerical Heat Transfer and Fluid Flow, Hemisphere, Washington, DC.
[14] Rhie, C. M., and Chow, W. L. (1983), "Numerical Study of the Turbulent Flow Past an Airfoil with Trailing Edge Separation," AIAA J., Vol. 21, No. 11, pp. 1525-1532.
[15] Majumdar, M. (1988), "Role of Under-relaxation in Momentum Interpolation for Calculation of Flow with Non-staggered Grids," Numerical Heat Transfer, Vol. 13, pp. 125-132.

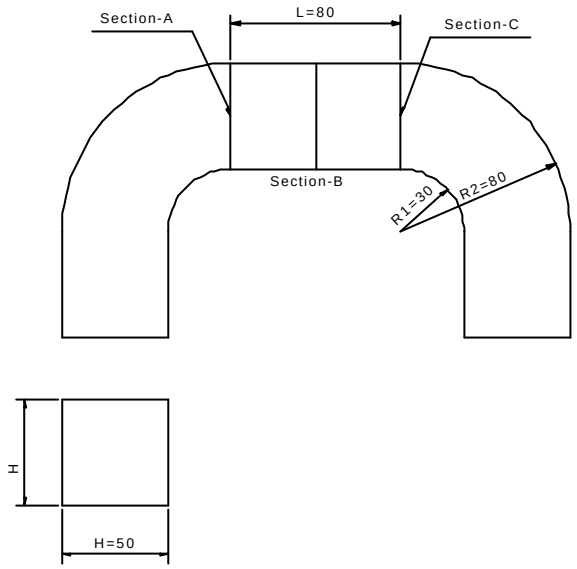

Fig.1 Geometry of curved duct.

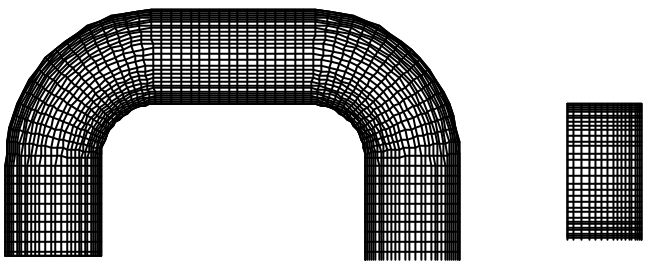

Fig.2 Grid distribution.

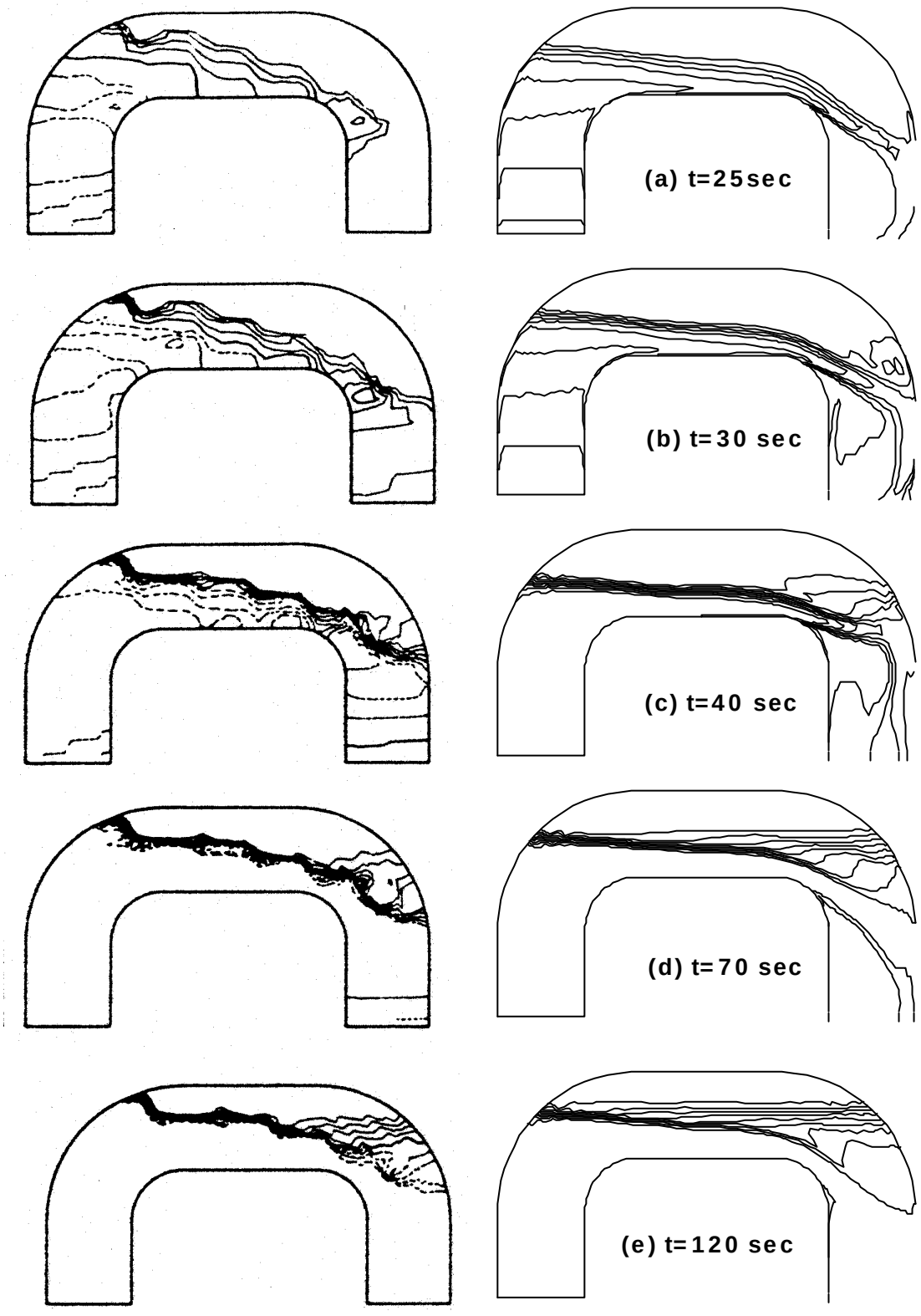

Fig.3 Comparision between experiments and calculated results of isotherms
(left : experimental results, right : calculated results).

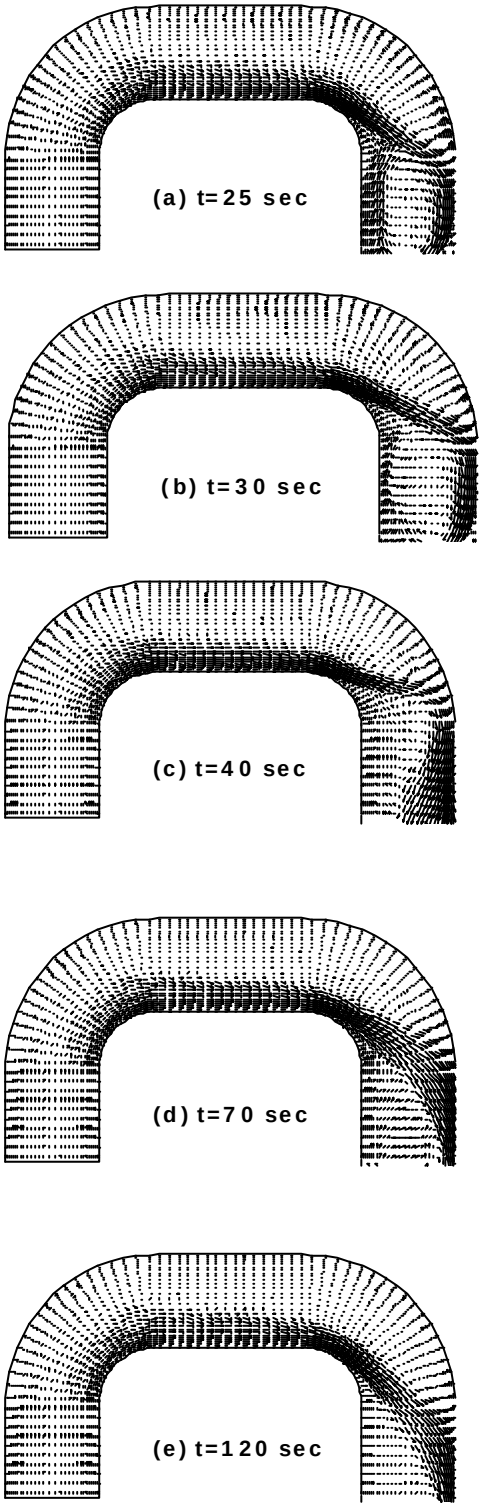

Fig.4 Predicted velocity vectors at the symmetry plane.

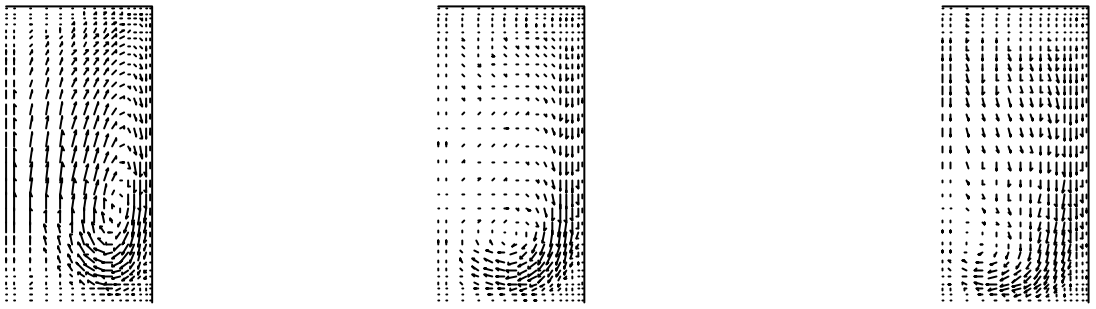

(a) t=0 sec

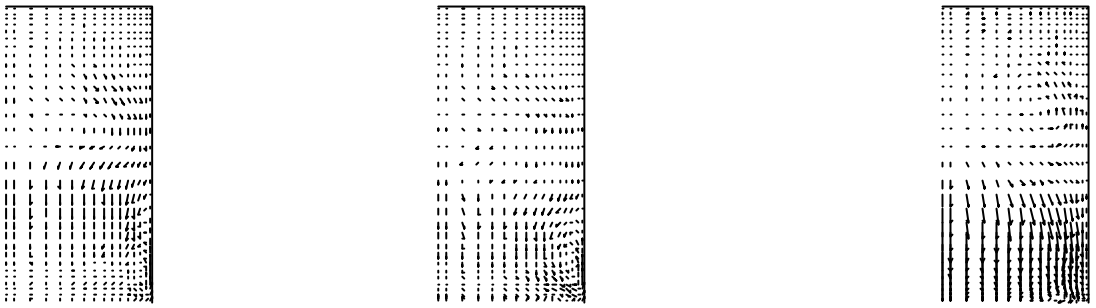

(b) t=25 sec

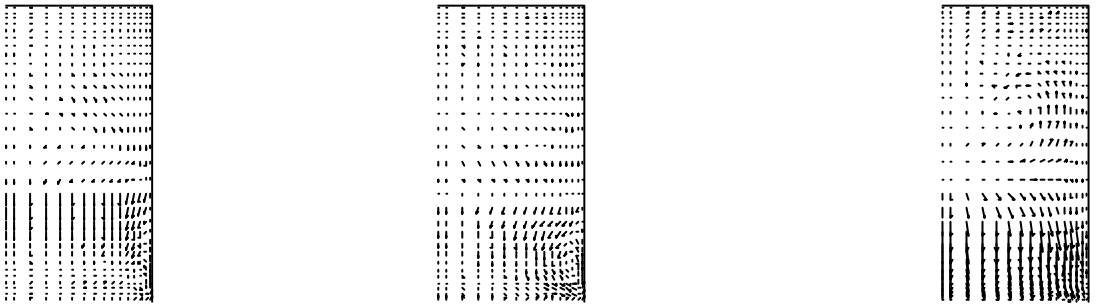

(c) t=30 sec

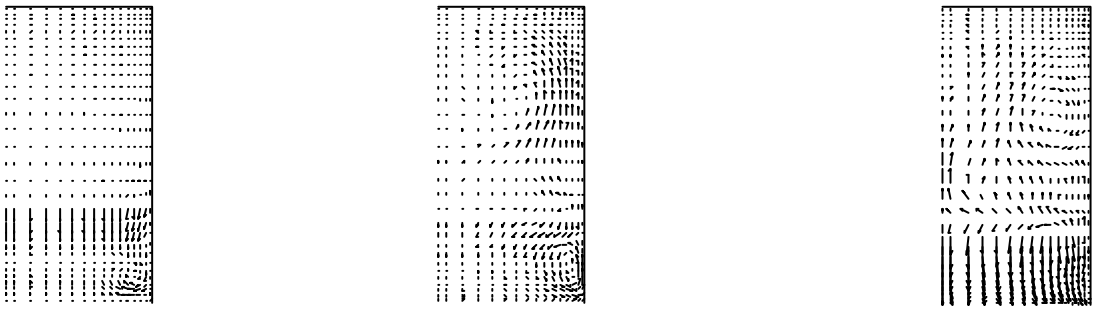

(d) t=40 sec

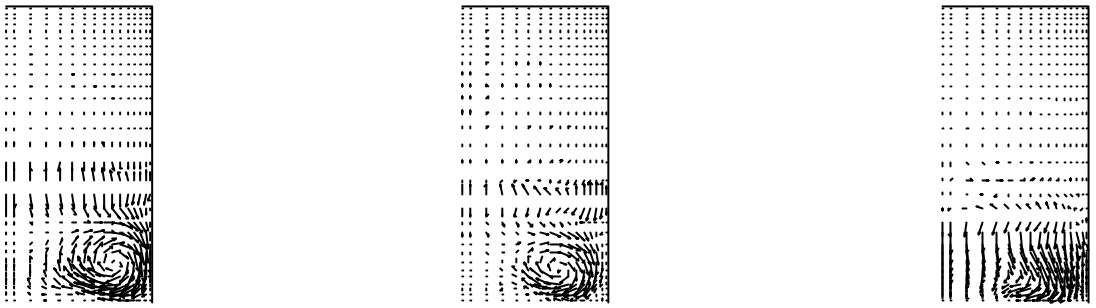

(e) t=70 sec

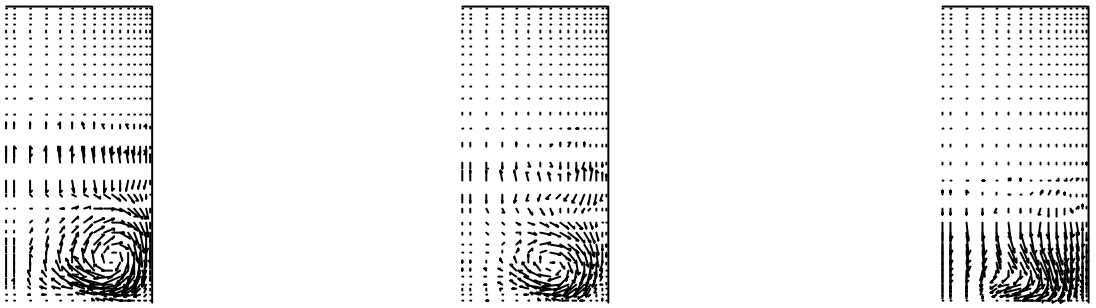

(f) t= 120 sec

Fig.5 Predicted secondary flow (left : section A; middle : section B, right : section C).

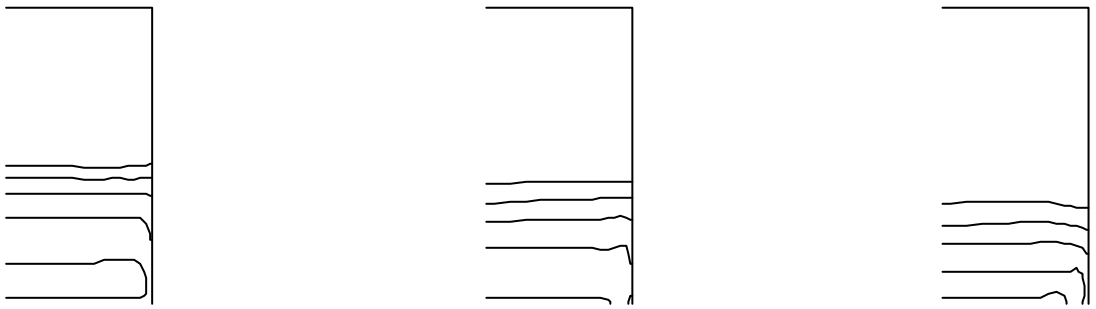

(a) t=25 sec

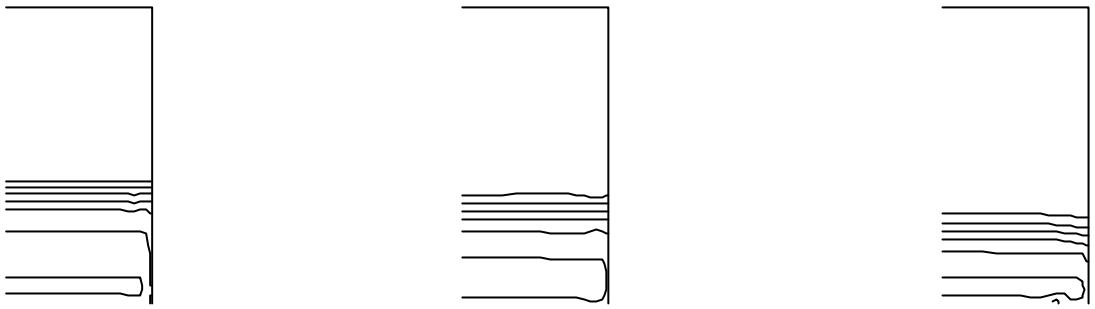

(b) t=30 sec

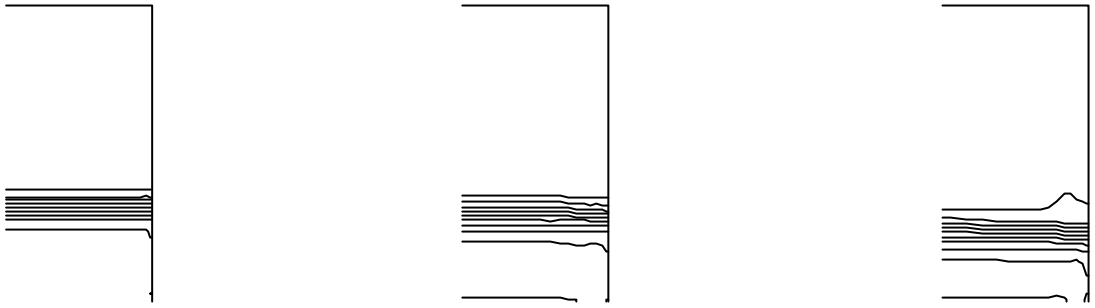

(c) t=40 sec

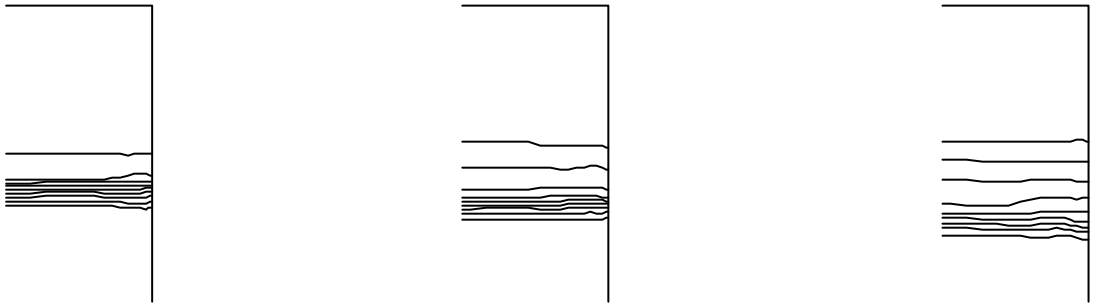

(d) t=70sec

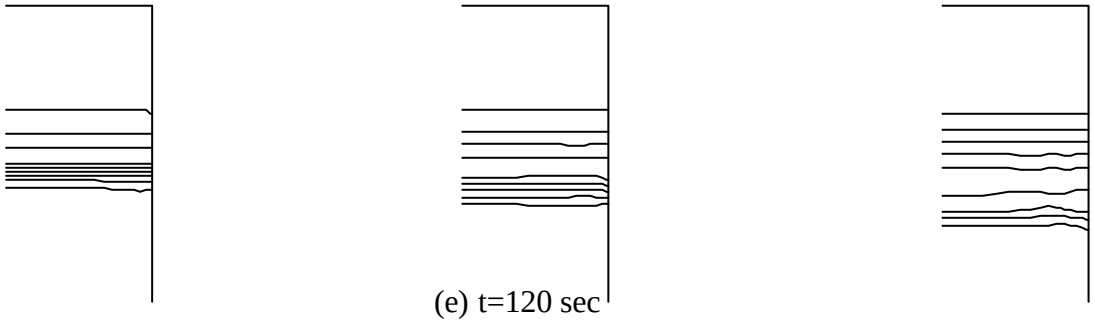

(e) t=120 sec

Fig.6 Predicted isothermal lines (left : section A; middle : section B, right : section C).